Relationship between interparticle contact lifetimes and rheology in gravity-driven granular flows

Robert Brewster,[1] Leonardo E. Silbert,[2] Gary S. Grest,[3] and Alex J. Levine[1,4]
[1]*Department of Chemistry and Biochemistry, UCLA, Los Angeles, California 90095, USA*
[2]*Department of Physics, Southern Illinois University, Carbondale, Illinois 62901, USA*
[3]*Sandia National Laboratories, Albuquerque, New Mexico 87185, USA*
[4]*California Nanosystems Institute, UCLA, Los Angeles, California 90095, USA*
(Received 6 August 2007; revised manuscript received 16 February 2008; published 11 June 2008)

The validity of the Bagnold constitutive relation in gravity-driven granular flow down an inclined plane is studied by discrete element (DEM) simulations. In the limit of infinitely hard particles, the Bagnold relation is known to hold exactly. We determine deviations from this relation as a function of all parameters governing interparticle interactions. These include elastic compliance, inelastic dissipation, friction coefficient, and interparticle cohesion. We find significant deviations from Bagnold rheology in some regions of this parameter space and propose a generalized Bagnold relation to account for this effect. Moreover, we note a significant correlation between the breakdown of Bagnold rheology in the bulk and the appearance of a long-time tail in the two-particle contact time distributions.

DOI: 10.1103/PhysRevE.77.061302 PACS number(s): 45.70.−n, 45.70.Mg, 83.10.Ff

I. INTRODUCTION

A successful "hydrodynamic" description of granular flows hinges on identifying appropriate constitutive relations between the local strain rate (and perhaps other variables such as density) to the local stress state of the system. With such a set of constitutive relations governing momentum transport through the system, it is then sufficient to include only the necessary conservation laws to develop a closed set of continuum relations to describe the flowing granular state at length scales large compared to that of the constituent particles.

Usually, granular flows can be characterized by the density, or packing fraction, of the bulk material. In dilute flows, particles typically undergo only binary collisions, and are transported with the mean, hydrodynamic flow, but also possess large velocity fluctuations that are of the same order of magnitude as the mean flow itself [1]. This type of flow can be modeled as a gas of inelastic particles using modified kinetic gas theories that include terms for the granular viscosity and granular temperature [2]. These typically lead to a local, linear relationship between the shear stress and rate of strain in the material. Slow, dense granular flows are often described as a quasistatic continuous medium that creeps via plastic deformations such that the flow properties are essentially velocity independent [3], whence the shear stress is proportional to the strain only.

For densities and excitations intermediate between these two regimes the flows are dense yet at the macroscopic scale, the material continuously deforms. At the same time, however, the stresses within the granular pile are dominated by contact forces so the Reynolds stress associated with the kinetic energy of the particles plays a subdominant effect [4]. This latter criterion is often used to differentiate between different flowing regimes. In the language of Campbell [5,6], here we investigate the *inertial–elastic-inertial* regime, using large-scale simulations of gravity-driven, dense granular flows down a rough and bumpy inclined plane.

Recent experiments [7–9], together with large-scale simulations [4], have focused much effort on the inclined plane geometry [10]. One common feature about these types of dense flows is that they are approximately described by Bagnold rheology [11]. The Bagnold relation posits that the shear stress in the system is proportional to the square of the rate of shear strain. In other words, the granular viscosity is linearly proportional to the local shear rate. Bagnold's argument for this relation as it applies to gravity-driven, inclined plane follows from the consideration that the transfer of down-plane momentum in the direction of flow (i.e., the x axis) perpendicular to the free surface (z) occurs via off-center binary collisions between hard particles. The frequency of these collisions and the magnitude of momentum transferred in each collision are both proportional to the shear rate $\dot{\gamma}$ so that the x-momentum flux through planes normal to the z axis is proportional to the square of the shear rate, or $\sigma_{xz} \propto \dot{\gamma}^2$.

The validity of the Bagnold constitutive law fundamentally relies on instantaneous binary intergrain collisions. It has been derived within the kinetic theory approach [12] applicable to rapid flows. Interestingly, as discussed by Lois *et al.* [13], the Bagnold constitutive law is a consequence of an exact symmetry of Newton's laws of motion for perfectly rigid spheres where interparticle forces become constraint forces to enforce mutual noninterpenetrability. Curiously, for hard spheres, the Bagnold constitutive relation will be exact in *all* flow regimes regardless of interparticle friction, and particle inelasticity. This picture seems to be corroborated by the inertial number constitutive model [14,15]. However, even hard spheres can exhibit deviations from Bagnold rheology at sufficiently high densities due to the emergence of correlated structures within the flow that modify the characteristic time scale of the system [16,17]. Shear flow simulations of soft spheres [18] also characterized different populations of colliding particles based on the duration of contacts. A number of rheological models that take into account various aspects of local and nonlocal effects have also appeared [19–24].

The current work was motivated by a recent study of cohesive granular materials where it was clearly shown that the Bagnold constitutive law fails [25]. These results suggest a more general question: What features of the intergrain interaction affect the continuum level description of momentum transport in the system? To examine this issue, we explore the complete parameter space of intergrain interactions to determine their effect on the continuum-level constitutive relation of the material. In this paper we study the rheological importance of the particles' elastic compliance, their coefficient of restitution (a measure of energy dissipation per collision), the magnitude of intergrain cohesive forces (e.g., due to a wetting fluid [26,27]), and the intergrain friction coefficient. We also compare between the Hookean and Hertzian contact force models. Finally, we vary the tilt angle of the granular system with respect to gravity in order to change the flow dynamics to observe their effect on the granular constitutive relation at least within the steadily flowing dense regime. In this way we seek to relate the fundamental physics of the intergrain interaction to the collective flow properties of the system as a whole. Rather than catalog the multiple rheological effects of varying multiple intergrain parameters, it would be clearly beneficial to identify a smaller set of microscopic variables that determine the collective behavior of the granular system.

The longevity of contacting pairs of particles emerges as a crucial parameter in the resulting flow properties and subsequent deviations from Bagnold rheology [28]. We have found that the most effective way to influence contact times is through tuning the elastic compliance of the particles, which can dramatically alter the rheology [28]. One approach to characterizing the quantitative importance of the particles' elastic compliance is through the Mach number $(=d\dot{\gamma}/2c$, where d is the particle diameter and c is the speed of sound in a grain). This ratio compares the sound propagation time across a granular particle to the inverse shear rate. It has been suggested that when this quantity is large one expects to observe larger deviations from simple Bagnold scaling [29]. However, the Mach number does not capture the complex and collective dynamics inherent to a many-body system such as large-scale granular flows.

We identify a more appropriate dimensionless parameter (a ratio of time scales) that correlates with the breakdown of the Bagnold rheology. In recent work [28], we attributed this breakdown to the formation of relatively long-lived clusters in the system. By spanning streamlines in the flow, these clusters allow for an additional momentum transport mechanism. This generates a term in the constitutive law proportional to $\dot{\gamma}$. To account for these two independent modes of momentum transfer, we proposed a modified constitutive relation of the form

$$\sigma_{xz} - \sigma_c = a\dot{\gamma}^2 + b\dot{\gamma}, \tag{1}$$

which allows for a combination of collisional and elastic momentum transport. Here, σ_c is the finite yield stress at the boundary between the liquidlike flowing region and the solidlike plug. This term is only nonzero when cohesive interactions are present. Based on this proposal, we suggested that the presence of long-lived contacts in the system plays the key role in determining the applicability of Bagnold's relation. When such long-lived contacts allow the formation of streamline-spanning clusters, the linear term in Eq. (1) will become significant resulting in the breakdown of the Bagnold hypothesis. By long-lived we mean that such structures endure over the typical period of particle rearrangements, which is set by the local shear rate.

In this paper we present new data on the intergrain contact time distribution and how variations in that distribution correlate with changes in the bulk rheology of the granular material. We find that any changes in the grain interaction parameters that lead to longer long-lived contacts do indeed lead to the failure of the Bagnold constitutive relation, i.e., the growth of the linear in the rate-of-strain term in Eq. (1). Additionally, we find that the typical intergrain interaction is always a simple two-body collision for any set of parameters. Thus, even in these dense flows where the particle volume fraction is about ten percent less than the random close-packed limit, the mean coordination number of the particles is approximately unity [28]. This counterintuitive result supports similar diffusion wave spectroscopy-based measurements on the densely flowing state by Menon and Durian [30]. Moreover, we find that we can correlate the granular rheology over our multidimensional parameter space of intergrain interactions with the duration of rare, long-lived contacts (to be defined precisely below), but not with the typical intergrain contact times. In all cases, the typical intergrain contact time remains short, however, it is the dynamics of the rare, long-lived intergrain contacts that control the collective bulk rheology of the material, leading to non-Bagnold behavior.

The remainder of this paper is organized as follows: We first review our simulation methods in Sec. II, followed by an exploration of the effect on granular rheology and interparticle contact lifetime distributions of varying specific interaction parameters in Sec. III. We then demonstrate that the lifetime of long-lived contacts controls the granular rheology in the densely flowing state and then summarize our results in Secs. IV and V, respectively.

II. SIMULATION METHOD AND DATA ANALYSIS

We present results for a series of discrete element simulations carried out on N monodispersed spheres of diameter d and mass m in three dimensions. The simulation area consists of a rough base with length $20d$, and width $20d$, tilted an angle θ with respect to gravity. We use periodic boundary conditions for both length (flow or x direction) and width (vorticity or y direction). For $N=35\,900$, as in most of our simulations, the height of the flowing pile is between $90d$ and $100d$ depending on the angle of inclination.

Our simulations use a modified version of the model developed by Cundall and Strack [31] and Walton [32] for the interparticle interactions. The inelastic contact forces are modeled through a spring-dashpot interaction for both normal and tangential forces to their line of centers. Consider two spheres i and j separated by $\mathbf{r}_{ij}=\mathbf{r}_i-\mathbf{r}_j$ with a relative velocity $\mathbf{v}_{ij}=\mathbf{v}_i-\mathbf{v}_j$. If they are in contact, the spheres have a relative normal compression $\delta_{ij}=d-|\mathbf{r}_{ij}|$, which results in a

normal and tangential component to the contact force $\mathbf{F}_{ij} = \mathbf{F}_{n_{ij}} + \mathbf{F}_{t_{ij}}$ with

$$\mathbf{F}_{n_{ij}} = f(\delta/d)\left(k_n \delta_{ij} \mathbf{n}_{ij} - \frac{m}{2}\gamma_n \mathbf{v}_{n_{ij}}\right) + \mathbf{F}_{ij}^c(\delta_{ij}), \tag{2}$$

$$\mathbf{F}_{t_{ij}} = f(\delta/d)\left(-k_t \mathbf{u}_{t_{ij}} - \frac{m}{2}\gamma_t \mathbf{v}_{t_{ij}}\right), \tag{3}$$

where $\mathbf{n}_{ij} = \frac{\mathbf{r}_{ij}}{|\mathbf{r}_{ij}|}$. The $k_{n,t}$ are elastic constants in the directions along (n) and tangential (t) to the line of centers. These parameters specify particle rigidity or elastic compliance. For example, the largest value used in these simulations, $k_n = 2 \times 10^9$ mg/d, roughly corresponds to a Young's modulus equal to that of glass spheres, $E \approx 6 \times 10^9$ Pa. Similarly, the $\gamma_{n,t}$ are dissipative constants that determine energy loss during collisions. The elastic tangential displacement $\mathbf{u}_{t_{ij}}$ is set to zero upon formation of a contact and is truncated as necessary to satisfy the Coulomb yield criterion, $|\mathbf{F}_t| \leq \mu |\mathbf{F}_n|$. The prefactor in Eqs. (2) and (3), $f(x)$, is unity for Hookean contacts (the force is proportional to the displacement) and $\sqrt{x}$ for Hertzian contacts (the force is proportional to displacement to the 3/2 power) [33]. $\mathbf{F}_{ij}^c(\delta_{ij})$ is the cohesive force, which is derived from an effective cohesive potential between particles i and j. This potential is modeled with a Gaussian well centered just inside the point of contact, $r_c = d - \ell$,

$$U_{ij}^c = -Ae^{-(r_c - |\mathbf{r}_{ij}|)^2/\ell^2}, \tag{4}$$

with an effective width $\ell = 0.01d$ leading to an adhesion force of the form

$$\mathbf{F}_{ij}^c = 2A\mathbf{n}_{ij}\frac{(r_c - |\mathbf{r}_{ij}|)}{\ell^2}e^{-(r_c - |\mathbf{r}_{ij}|)^2/\ell^2}. \tag{5}$$

The short-range cohesive force is set to zero for distances greater than $1.02d$. This simple form is chosen for the cohesive force on the criterion that it is short ranged, the magnitude is easily controllable (through A), and the form is computationally simple [25]. For the majority of this work we study cohesionless particles $(A = 0)$.

In a gravitational field the total force on the ith particle is determined by

$$\mathbf{F}_i^{\text{tot}} = m_i \mathbf{g} + \sum_j (\mathbf{F}_{n_{ij}} + \mathbf{F}_{t_{ij}}), \tag{6}$$

where the sum extends over all particles j in contact with the ith particle and $\mathbf{g}$ is the acceleration due to gravity.

Energy dissipation occurs during collisions due to the velocity dependent forces in Eqs. (2) and (3). Additionally the work done in creating elastic strains $\mathbf{u}_t$ at an established interparticle contact is lost with either interparticle slip at the Coulomb criterion or particle separation. For Hookean contacts the coefficient of restitution, e_n, parametrizes the dissipative nature of the interparticle collisions. In terms of the parameters introduced in Eq. (2) for Hookean contacts,

$$e_n = e^{(-\gamma_n t_{\text{col}}/2)}. \tag{7}$$

Here, t_{col} is the duration of an interparticle contact during a collision between two particles—the binary collision time—which is given by

$$t_{\text{col}} = \frac{\pi}{\sqrt{(2k_n/m - \gamma_n^2/4)}}. \tag{8}$$

For Hertzian contacts we still parametrize energy dissipation during interparticle collisions using γ_n, but cannot define a coefficient of restitution because the energy loss depends on the relative velocity between the particles.

We varied most of these interaction parameters during this study. Unless otherwise stated, we set $k_t = 2k_n/7$, $\mu = 0.5$, and $\gamma_t = 0$. In the Hookean case, when varying k_n, γ_n is also varied to maintain a fixed coefficient of restitution, $e_n = 0.88$ (unless another value is explicitly stated). For example, $k_n = 2 \times 10^5$ mg/d, requires $\gamma_n = 50\tau^{-1}$ to ensure the desired coefficient of restitution. We used these same values of $k_{n,t}$ and $\gamma_{n,t}$ for the Hertzian contacts. All times are reported in units of τ, where $\tau = \sqrt{d/g}$. The time step for all simulations with $k_n \leq 2 \times 10^5$ mg/d is $\delta t = 10^{-4}\tau$. To ensure accurate integration of the dynamics, the time step was reduced with increasing spring constant. For $k_n = 2 \times 10^6$ mg/d we set $\delta t = 2.5 \times 10^{-5}\tau$, $k_n = 2 \times 10^7$ mg/d, $\delta t = 1 \times 10^{-5}\tau$, and $k_n = 2 \times 10^9$ mg/d, $\delta t = 1 \times 10^{-6}\tau$. The initial system was allowed to evolve for up to $10^9 \delta t$. In the steady state, data was collected over a period of $2-5 \times 10^6 \delta t$.

To determine the extent to which the flow field satisfies that expected from the Bagnold constitutive law we examine the velocity profile $v_x(z)$ in the chute flow geometry at an inclination angle θ. By symmetry the only nonzero strain rate and velocity in the system are $\partial_z v_x$ and v_x, respectively. The solution for the granular flow with a free surface at height $z = h$ is determined by requiring force balance $\partial_z \sigma_{xz} + \rho g \sin\theta = 0$, where ρ is the mass density of the pile.

$$v_x(z) = \frac{2a}{3c}\left[\left(G^2 + \frac{ch}{a}\right)^{3/2} - \left(G^2 + \frac{c}{a}(h - z)\right)^{3/2}\right] - Gz, \tag{9}$$

where $c = \rho g \sin\theta$ and $G = \frac{b}{2a}$. When cohesive interactions are present, the yield criterion from Eq. (1) is included and h is the height of the flowing pile beneath the solid plug. The constants a, b from Eq. (1) are not known *a priori*. These values are adjusted to achieve the best fit to the velocity profile data using an implementation of the nonlinear least-squares (NLLS) Marquardt-Levenberg algorithm. The solution given in Eq. (9) assumes a spatially uniform mass density in the system. This assumption was directly tested against the simulation data in the flowing regime and was found to be valid except near the upper surface. For cohesionless systems, this consists of a saltating layer near the free surface a few layers thick. For cohesive flows, this corresponds to the solid plug region where $\dot{\gamma} \approx 0$. The solid plug is of higher density than the flowing, dilated region below. No data for particle contact dynamics or granular rheology was taken from either of these regions.

Of more physical relevance is the ratio of the stress contribution from the term linear in $\dot{\gamma}$ to that from the quadratic term. This ratio is defined by

$$\Omega = \frac{b\dot{\gamma}}{a\dot{\gamma}^2}. \tag{10}$$

This will be used throughout this work to characterize the deviation of a flow from the traditional Bagnold constitutive relationship. $\Omega=0$ corresponds to a purely Bagnold flow with a viscosity proportional to $\dot{\gamma}$, and $\Omega\to\infty$ corresponds to a completely non-Bagnold flow with viscosity independent of $\dot{\gamma}$. In the following we explore particle interaction parameters that cause deviations.

Based on our previous work on the effects of granular cohesion of flow rheology, we believe that the principal cause of the breakdown of Bagnold rheology in this case is the formation of long-lived interparticle contacts in the material. Here we examine whether the presence of such long-lived contacts is the generic cause of the breakdown of Bagnold rheology in granular systems.

To meaningfully define a contact time and thus give a precise definition to "long-lived contact" we compare interparticle contact times τ_c, to the typical time scale for particle rearrangements in the flowing state. That time scale is set by the shear time $\dot{\gamma}^{-1}$. Throughout this work, we use the dimensionless quantity given by the ratio of the contact time to the shear time, $\tau_c\dot{\gamma}$, measured locally in the flow. Because of the depth dependence of the flow velocity, we choose to compare lifetimes and their distributions at the center of the flowing pile. Though this choice is arbitrary, the average contact lifetimes [see Fig. 4(b)] are relatively insensitive to position in the flowing pile.

To analyze the failure of Bagnold rheology we compute not only the deviation from Bagnold rheology via Ω, but also the distribution $P(\dot{\gamma}\tau_c)$ of dimensionless contact times $\dot{\gamma}\tau_c$, where τ_c is the time that two particles remain in continuous contact. Two particles are considered in contact as long as they remain within a distance d_c of each other. For Secs. III A and III D, where the cohesive force is not present, $A=0$, we use $d_c=d$, which is to say that a contact is considered broken once two particles no longer physically touch. In the case of cohesive particles, we take the contact zone to be extended beyond d since the cohesive force continues to act on neighboring particles even when physical contact is broken. We will discuss this further in Sec. III E. The contact zone can also be widened to allow for high frequency rattling, which may not be detectable in experiment. A comparison of $P(\tau_c)$ for $d_c=d$, $1.001d$, $1.01d$, and $1.02d$ is shown in Fig. 1 for a noncohesive system. As seen from this figure, a general decrease in contact times is seen as d_c approaches d exactly. We will return to discuss these features further in Sec. III E.

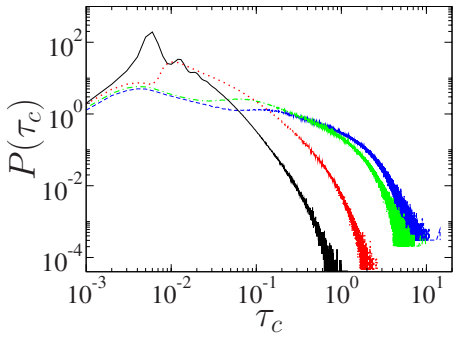

FIG. 1. (Color online) Contact lifetime distributions $P(\tau_c)$ for Hookean particles in the center of the pile with $\theta=23°$ and $k_n=2\times10^5$ mg/d for values of $d_c=d$ (black solid), $1.001d$ (red dotted), $1.01d$ (green dash-dotted), and $1.02d$ (blue dashed). The main features are the shrinking of the short contact time peak associated with binary collisions and the growth of the long contact time tail as the contact zone is widened.

III. RESULTS

We now systematically modify properties of the interparticle interaction and monitor their effect on granular rheology and the distribution of contact times in the material. Several parameters of the granular system are found to have significant influence on both the flow profile and the contact time distributions.

A. Particle hardness

As expected from general principles the stiffness of the particles plays a dramatic role in controlling deviations from Bagnold rheology. We begin by examining the effect of changing particle spring stiffness.

To accurately model a hard-particle material such as glass beads of size $d=100$ μm and density 2500 kg m^{-3}, a spring constant of order 10^{10} mg/d is needed. Such large elastic constants require a computationally prohibitive reduction in the size of the integration time step. Consequently, past simulations have used spring constants $k_n\sim\mathcal{O}(10^5)$ mg/d to capture the behavior of hard-particle systems [4,12,34,35]. The quantitative effect of the particles' elastic compliance on the granular rheology has been reported elsewhere [28].

In Fig. 2 we plot Ω, as defined in Eq. (10), vs the effective spring constant k_n of the particles in order to quantify deviations from Bagnold rheology. Here the particles interact via

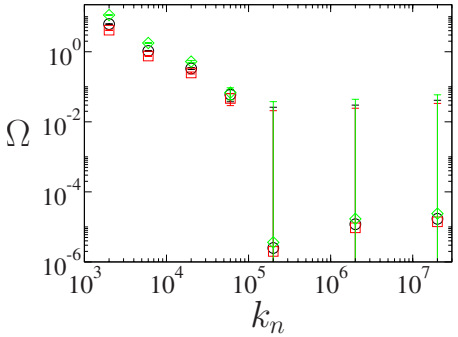

FIG. 2. (Color online) Ω vs k_n (in units of mg/d) for Hookean particles with $e_n=0.88$ at three different heights z within the pile (red $\square$ for $z=\frac{h}{4}$, black $\bigcirc$ for $z=\frac{h}{2}$, and green $\diamond$ for $z=\frac{3h}{4}$). Ω is large for small values of k_n but goes toward zero as the particles stiffness increases.

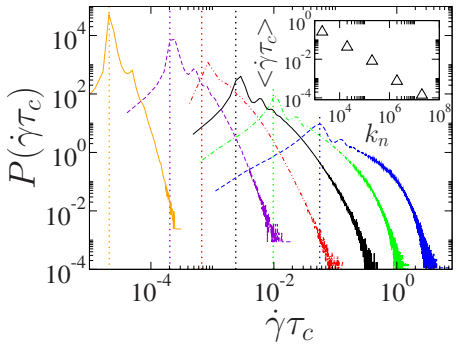

FIG. 3. (Color online) Contact lifetime distributions $P(\dot{\gamma}\tau_c)$ for Hookean particles in the center of the pile with $\theta=23°$. The figure shows distributions for several values of k_n, which read from right (small k_n) to left (large k_n) on the figure; $k_n=2\times10^3$ mg/d (blue dashed), 2×10^4 mg/d (green dash-dotted), 2×10^5 mg/d (black solid), 2×10^6 mg/d (red dash-double dotted), 2×10^7 mg/d (violet dashed), and 2×10^9 mg/d (gold solid). $P(\dot{\gamma}\tau_c)$ is scaled down for $k_n=2\times10^7$ mg/d and 2×10^9 mg/d, by 10 and 10^5, respectively. Vertical lines represent the two-body collision times. The inset shows the average contact time as a function of k_n. The contact lifetime is nondimensionalized by the shear rate at the midpoint of the pile.

Hookean springs and γ_n is varied so that the coefficient of restitution $e_n=0.88$ for all seven values of k_n. Since $\dot{\gamma}$ depends on z, we show Ω for three distinct heights within the pile: $z=\frac{h}{4}$, $z=\frac{h}{2}$, $z=\frac{3h}{4}$. As expected we note the general trend that lower particle elastic compliance leads to a more Bagnold-like constitutive relation at all measured heights. Indeed, our data for $k_n\geq2\times10^5$ mg/d is consistent with $\Omega=0$, i.e., with the Bagnold constitutive relation. For more compliant particles, however, there is a significant deviation from Bagnold rheology. As the spring constant k_n decreases, the linear momentum transport term becomes more important in describing the flow profile. For the softest spring constant studied, the linear in shear rate term in the constitutive law accounts for more than four times the stress than does the Bagnold contribution. Examining the entire data range we find that the empirical relation

$$\Omega \simeq J\left(\frac{dk_n}{mg}\right)^{\beta}, \tag{11}$$

holds well at a fixed height within the pile using the parameter values $\beta=-1.3$, and $J=1.25\times10^5$. The value of Ω depends not only on k_n, but also on the local shear rate.

In Fig. 3 the contact lifetime distribution in the center of the pile is shown for several values of k_n. The peak at short times coincides well with the calculated collision time $\dot{\gamma}t_{\mathrm{col}}$, which is shown by the vertical lines in the figure. This line represents the contact time of a simple two-body collision between underdamped Hookean springs; the time they spend in contact will be half of one period of oscillation [Eq. (8)]. The contact lifetime distributions are clearly dominated by the weight of the binary collision peak. However, as the particles become softer, the weight of this peak decreases and the distribution becomes broader. For $k_n<10^5$ mg/d, there is an increasing fraction of long-lived particle contacts with $\dot{\gamma}\tau_c=\mathcal{O}(1)$. These excessively long-lived contacts in the softer particle systems appear to promote the formation of transient stress-bearing structures within the material. These structures span streamlines in the flow thus elastically transmitting stress across their length in proportion to the rate of particle impacts with these structures, which occur at a rate $\sim\dot{\gamma}$.

The mean contact lifetime as a function of spring constant is shown in the inset of Fig. 3. The average dimensionless contact lifetime $\langle\dot{\gamma}\tau_c\rangle$ decreases with increasing k_n by several orders of magnitude over the range of k_n. The average contact lifetime simply scales as the two-body collision time $\langle\tau_c\rangle\sim k_n^{-1/2}$. This shows that the mean contact lifetime is dominated by the two-body collision peak and is relatively insensitive to the changes in the long-time tail of the contact time distribution. In Sec. IV, we discuss the proper scalar representation of the contact distribution and compare it with our scalar value for rheology change, Ω.

B. Hookean vs Hertzian contacts

Both the linear Hookean and nonlinear Hertzian force-displacement laws are commonly used to model granular particles. The Hertz contact law is more suitable in taking into account surface deformations that occur during collisions between elastic spheres [33]. In fact, Hertz contact forces are often necessary to accurately describe phenomena involving elastically compliant particles, e.g., understanding the propagation of sound in bead packs [36]. Here we compare the granular rheology and contact lifetime distributions for these two force laws to study their similarities and distinctions.

The contact lifetime distribution data shown in Fig. 4 are for Hookean and Hertzian contacts with $k_n=2\times10^4$ mg/d and 2×10^5 mg/d. All other parameters are identical. The main feature is an overall increase in average contact lifetime for the Hertzian contacts at any given height within the pile for a particular value of k_n, highlighted in Fig. 4(b).

Based on our intuition that longer contact times lead to particle structures that transmit stress elastically across the system, we expect the rheology to be less Bagnold-like for Hertzian contacts showing an increased weight of the term linear in $\dot{\gamma}$. Figure 5 shows the effect of changing from Hookean to Hertzian potentials to model the interparticle forces. We show data for Ω only from the middle of the pile ($z=\frac{h}{2}$), although the same behavior is observed anywhere in the bulk. For Hertzian contacts with $k_n=2\times10^3$ mg/d, $\Omega\simeq10^4$ consistent with a simple linear relation between stress and strain rate within our numerical precision (data not shown). In general, for all values of the spring constants, Hertzian flows indeed conform less to the Bagnold prediction. This result is intuitively reasonable because Hertzian springs are "softer" for small compressions, which will promote longer contact times. It is worth noting the similarities in contact lifetime distributions of Hookean contacts with $k_n=2\times10^4$ mg/d (black dashed) and Hertzian contacts with $k_n=2\times10^5$ mg/d (red dash-dotted) in Figs. 4(a) and 4(b) and comparatively similar rheology as measured by Ω in Fig. 5. The striking point is that the details of the interaction do

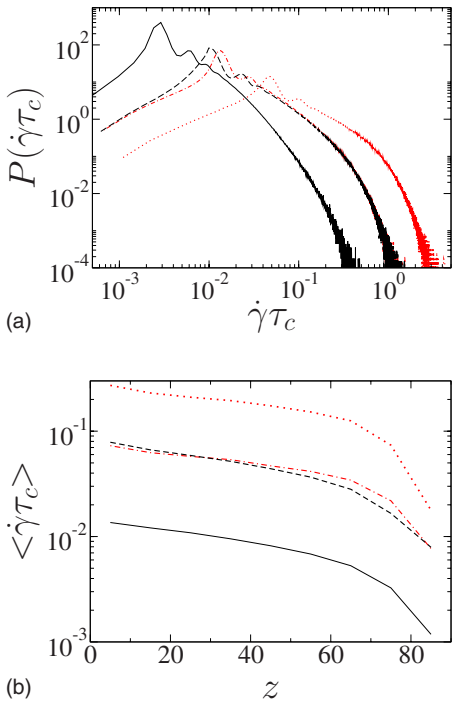

FIG. 4. (Color online) (a) Contact lifetime distributions for Hookean and Hertzian contact force laws with inclination angle $\theta=23°$ using (i) $k_n=2\times10^5$ mg/d (Hookean: black solid; Hertzian: red dash-dotted) and (ii) $k_n=2\times10^4$ mg/d (Hookean: black dashed; Hertzian: red dotted). In (b) the average dimensionless contact time vs height in pile (z) is shown using the same symbols as in (a). The average contact lifetime for Hertzian particles is consistently longer than for the Hookean particles, all other parameters being equal.

not appear to matter; if the contact distribution is similar, one should expect similar rheology and vice versa.

The flows corresponding to both of these force laws behave as expected when k_n gets very large or very small. However, it is important to note that if one is interested in modeling granular flows for hard particles, it is vital to use large $k_n \gtrsim 10^6$ mg/d in order to avoid possible artifacts that

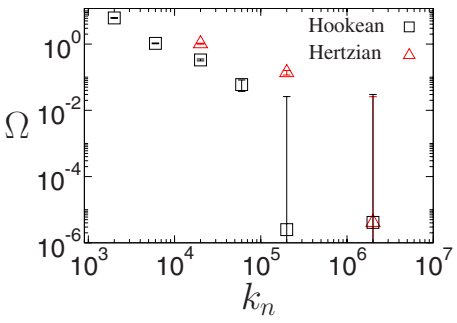

FIG. 5. (Color online) Comparison of Ω vs k_n for Hertzian (red $\triangle$) and Hookean (black $\square$) particle simulations for inclination angle of $\theta=23°$. Hertzian contacts display a greater deviation from the pure Bagnold constitutive relation for all values of k_n. For $k_n=2\times10^3$ mg/d the Hertzian particles are highly non-Bagnold, $\Omega>10^4$ (not shown) and the linear term completely dominates the constitutive relation.

may arise from using particles that are too soft. Particles with Hookean contacts, on the other hand, have a larger regime of effectively Bagnold rheology and thus allow simulations at smaller spring constants to reproduce physical flows of much harder particles.

C. Coefficients of restitution and friction

The dissipative properties of the interparticle interactions also have effects on the distribution of contact lifetime in the flowing pile. The effect of energy dissipation in collisions, as parametrized by the coefficient of restitution e_n, has been proposed to play an important role in some models of inclined plane flows [37]. In addition one may inquire as to the effect of the friction coefficient μ on granular rheology. We find, however, that changing either e_n or μ has a generically small effect on the contact time distribution and a correspondingly small effect on the granular rheology. This is attributed to a competition in time scale behavior that is not present in Sec. III A or Sec. III B.

In the previous sections on the effect of k_n on flow behavior, γ_n was varied in order to keep the coefficient of restitution at the constant value of $e_n=0.88$. We now fix the spring constant for Hookean interactions at $k_n=2\times10^4$ mg/d and vary γ_n to examine the effect of varying e_n [see Eq. (7)] on particle contact lifetimes and granular rheology. On decreasing e_n one might expect an increase in contact lifetimes by removing more energy per collision during the flow. However, the internal time scale $\dot{\gamma}^{-1}$ also increases as more energy is removed from the system in collisions. Examining the upper panel of Fig. 6 we note that decreasing the coefficient of restitution has a very small effect on the contact lifetime distribution and on the mean contact time (inset) when scaled by the shear time. This change is less dramatic than that due to changing the elastic compliance of the particles as shown in Fig. 3. The competing effects of longer contact times and an increase of the internal time scale largely balance when changing e_n. We return to these data and discuss one method of quantifying the rheological changes in Sec. IV.

Increasing the friction constant μ allows particles in contact to store more elastic energy in those contacts before slipping at the Coulomb criterion. By preventing slipping until larger total strains, one would expect an increase in μ to lead to longer-lived contacts. This effect may be dramatic if contacts are predominantly of the sliding type. If, however, most contacts are actually transient collisions or rolling contacts, one might expect the effect of changing μ to be rather minimal. The lower panel of Fig. 6 shows the contact time distribution for a variety of friction coefficients between $0.2\leq\mu\leq0.5$. The inset to the figure shows the dependence of the mean contact lifetime on μ. The binary collision peak is prevalent in each data set; because μ can have no effect on the binary collision time the position of these peaks differ only by $\dot{\gamma}$. The long contact time tail is remarkably similar for each distribution. This similarity suggests that long-lived contacts are of the sliding variety. As μ is increased, the shear time also increases; Fig. 6(b) suggests that in the tail of the distribution the increase in the shear time is balanced by an increase in the duration of long-lived contacts. These contacts cannot, then, be of the rolling type.

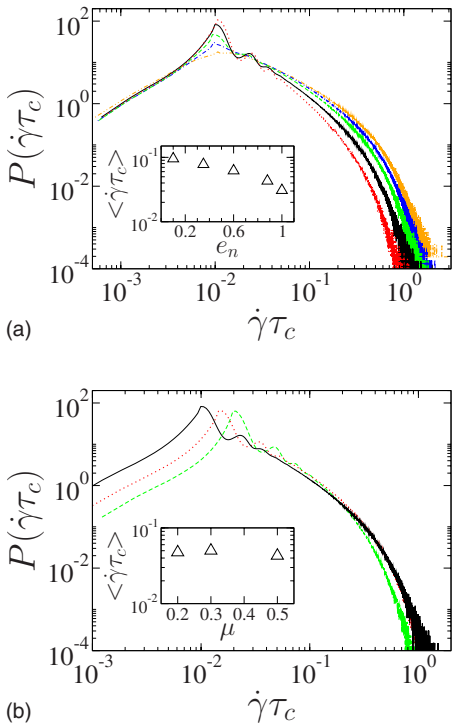

FIG. 6. (Color online) Contact lifetime distributions with $k_n = 2\times10^4$ mg/d for (a) e_n=0.10 (gold double-dot dashed), 0.35 (blue dash-dotted), 0.60 (green dashed), 0.88 (back solid), 1.0 (red dotted), and (b) μ=0.2 (green dashed), 0.3 (red dotted), and 0.5 (black solid). The tails of the contact time distributions do not show large dependence on either parameter. The insets show the dependence of the mean contact lifetime on e_n and μ, respectively.

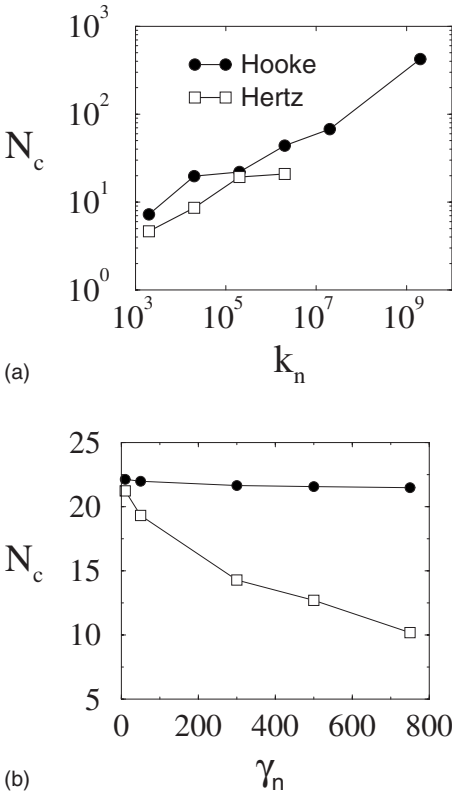

FIG. 7. Dependence of the collision rate N_c on (a) k_n, with μ =0.5 at fixed dissipation (e_n=0.88 for the Hookean system), and (b) γ_n, with μ=0.5 at fixed $k_n = 2\times10^5$ mg/d, for both the Hookean and Hertzian force laws flowing at θ=23°.

In the case of k_n and force law choice, the observed dimensionless contact times differ by orders of magnitude. In the case of the dissipative coefficients, e_n and μ, there is no change of such a magnitude. As expected, there is also no large change in rheology associated with variations of these parameters. Small changes in the dimensionless contact times are difficult to resolve because data is collected from a slice of finite width within the pile where the shear time is treated as constant over this range. In this analysis there is a balance between choosing a large enough region of the pile over which to report contact distributions with reasonable statistics, and choosing a thin enough slice of the pile so that the shear time does not vary dramatically over the sample. In spite of these constraints, we can say with certainty that the dependence of both the contact time distribution and the rheology on k_n and choice of force law is far stronger than that of the dissipation due to μ and e_n.

We have also studied the influence of particle stiffness and restitution coefficient on collision rates. In Fig. 7 we show the collision rate N_c defined as the average number of collisions per particle per τ, for a range of parameters. The strongest dependence comes from k_n shown in Fig. 7(a), where N_c increases as a weak power law of k_n with power-law exponent ~0.25, for both Hookean and Hertzian force laws. This dependence quantifies the increasing weight of the binary collision peak in the lifetime distributions shown in Fig. 3 and is consistent with a divergence toward an inelastically collapsed state in the hard sphere limit [38], similar to other two-dimensional studies [39], where a power-law exponent of ~0.4 was observed.

These results show that despite the growing collision rate and the propensity for hard particles to approach inelastic collapse, the rheology, as quantified in Figs. 2 and 5, is accurately described by the Bagnold law in the hard sphere limit as discussed by Lois *et al.* [13]. This raises some interesting questions regarding the underlying physical mechanisms that lead to deviations from Bagnold rheology. These results suggest the following picture, which is the focus of current research [40]: The majority of the stress in the system arises from the interaction forces between particles in contact. These contact stresses can be decomposed into a binary-collisional component, whereby contact stresses are transmitted over time scales short compared to the shear deformation time, and a long-lasting contact component, whose contacts survive appreciably longer, which allows stresses to be transmitted along extended particle structures across streamlines in the flow. The ratio of these two pieces of the contact stress is fundamental in determining the rheology of a granular system. Similar ideas have been explored in two-dimensional simulations of periodic shear flows of hard spheres [16,17,41] and confined soft spheres [18].

D. Dependence on tilt angle

If the key rheological control of the flowing state is the duration of long-lived contacts measured in units of the shear

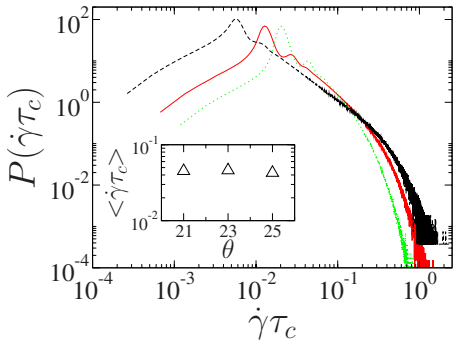

FIG. 8. (Color online) Contact time distributions for three values of tilt angle $\theta=21°$ (black dashed), 23° (red solid), and 25° (green dotted) for Hertzian contacts and $k_n=2\times10^5$ mg/d. Inset: dependence of contact time on θ.

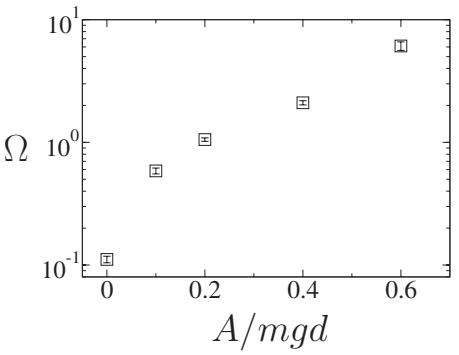

FIG. 9. Ω vs A for Hookean particles with $k_n=2\times10^5$ mg/d, total height $200d$. $\dot{\gamma}$ is measured at the center of the pile. A has a drastic effect on the rheology of the system as the system moves further from Bagnold rheology as the strength of the cohesive attraction is increased.

time, then it should be possible to also vary the dynamics of the system by directly varying the shear time while keeping the microscopic interaction parameters fixed. We do this by changing the inclination angle of the plane. An increase in the tilt angle θ, will increase the shear rate in the pile, which leads to a decrease in the shear time; all collisions appear longer to the system. Changing the tilt angle may, however, have other effects on the particle contact time distribution, since at higher tilt angles the grains have larger kinetic energy and higher granular temperature (velocity fluctuations) which might lead to the breakup of long-lived contacts. Tilting the pile will result in a decrease of the shear time and perhaps a decrease in the statistical weight of the long-lived contacts in the contact time distribution. Depending on which effect dominates, we can expect an increase in θ to result in a less Bagnold-like flow if the shear time effect dominates or a more Bagnold-like flow if the temperature effect dominates.

Figure 8 shows data for three values of θ for Hertzian contacts with $k_n=2\times10^5$ mg/d. In considering these contact time distributions with varying θ it is important to recall that for Hookean contacts the collision time of the particles is independent of their incoming velocity so the two-body collision time does not change with θ. For Hertzian contacts, however, the two-body collision time increases with increasing incoming velocity so in this more physically relevant system there should be an increase in the fundamental collision time in the system.

When changing the angle of inclination, each distribution has the same characteristic shape. The peak in each distribution, which we have seen corresponds closely with the two-body collision time moves toward shorter times as the tilt angle increases. This is consistent with the trend predicted by the scaling of two-body collision times for particles having Hertzian interactions. We see that the competition between the two relevant time scales results in only minimal changes in the scaled contact time distribution; for larger values of θ both the shear time and the average contact time are decreasing. We thus expect there to be only a small rheological effect associated with changing angle. This angle independence is encouraging for the existence of an effective continuum-level constitutive law for dense flowing granular materials. If, on the other hand, there had been a significant effect of tilt angle on the appropriate constitutive relation, there would be little meaning for such a local stress strain relation since any putative relation would also depend on the global geometry of the flow.

This analysis can be performed only in the steady-state regime of the chute flow so the range of available angles is confined by the lower and upper bounds of $\theta_i<\theta<\theta_{\text{free}}$. Below this lower bound $\theta_i=20.5°$ the flow is intermittent [42]. Above the angle of $\theta_{\text{free}}=27°$ the particles freely accelerate down the chute indefinitely and no steady-state regime exists. Given this limitation on the range of θ and thus the scale of the imposed shear rate, it is reasonable to conclude that tilt angle has little effect on the contact time distribution or the granular rheology (data not shown). It is quite possible that for taller piles or for more compliant particles one of the two effects would dominate and measurable deviations with changing θ would then be observed.

E. Interparticle cohesion

In previous work we reported on the breakdown of Bagnold rheology in cohesive granular material where the intergrain interactions incorporate the cohesive force shown in Eq. (5) [25]. The departure from the Bagnold constitutive law was attributed to the presence of momentum transport through extended structures of particles remaining in contact. We now study the contact lifetime distribution and rheology of such cohesive systems in more detail. In Fig. 9, we plot Ω as a function of the strength of the cohesive interaction A, for system of $k_n=2\times10^5$ mg/d and total height $\approx200d$ (the height of the flowing region h depends on the cohesive strength). Intergrain cohesion has a drastic effect on the rheology, on par with the effects seen for varying the spring constant k_n as seen in Sec. III A. We also observe the expected trends: increasing the cohesive strength increases the importance of the linear term in the modified constitutive law. Even in the case of very hard particles, the cohesive interaction allows the linear term to dominate the overall constitutive relation.

We should expect, then, to observe a correspondingly large increase in the number of extremely long-lived con-

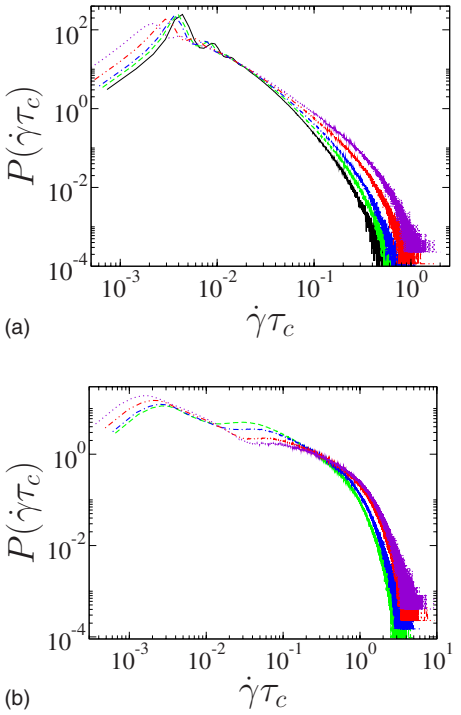

FIG. 10. (Color online) Contact lifetime distributions $P(\dot{\gamma}\tau)$, using Hookean contacts with $k_n=2\times10^5$ mg/d and $\theta=23°$ for $A=0.0$ (black line), $A=0.1$ (green dashed), $A=0.2$ (blue dash-dotted), $A=0.4$ (red double-dot dashed), and $A=0.6$ (violet dot) for (a) $d_c=d$, and (b) $d_c=1.02d$ for contacts in the middle of the flowing pile, $z=h/2$. When $d_c=d$ as in (a), increasing the strength of the cohesive interaction does not drastically change the width of the exponential tail. (b) shows the result of widening the contact criterion to include the extra width from the cohesive interaction.

tacts. Figure 10(a) shows the contact time distribution for several values of the cohesive strength using $d_c=d$. It is initially puzzling to note that the effect of A on the contact time distribution is rather weak, given that interparticle cohesion is a significant rheological modifier. As seen in Fig. 9, the rheology of the system depends quite strongly on this parameter. This discrepancy presents a problem.

In the previous sections where $A=0$, two particles were considered to be in contact only if the separation of their centers was equal to or less than one diameter, so that they could exert forces on each other. Clearly, when $A>0$, particles can interact over a larger range of $1.02d$; the range of the attractive force. Since we are interested in interparticle contacts inasmuch as they serve to transport momentum through the system, our definition of particle contact must be extended to include particles separated by $1.00d<d_c<1.02d$ that exert only cohesive forces on each other. However the adhesive contact potential at separations near $1.02d$ generates vanishingly small forces, while the typical contact forces make up a significant fraction of the weight of a particle. Thus, we extend the contact zone to include the range over which pairs maintain significant (i.e., at least mg in magnitude) interactions. We introduce an *effective contact range* d_{eff} defined by

$$mg = 2A\frac{(r_c - d_{\text{eff}})}{\ell^2}e^{-(r_c - d_{\text{eff}})^2/\ell^2}. \tag{12}$$

As the overall scale of the adhesive force increases (with increasing A) the effective contact range grows from $1.00d$ ($A=0$) to $1.014d$ ($A=0.6$). For very small values of the cohesion [$A=\mathcal{O}(10^{-2})$], Eq. (12) has no solution and the magnitude of the cohesive force is always less than the weight of one particle. In this case, the cohesive force is never significant as compared to the magnitude of contact forces and the contact zone is simply $d_{\text{eff}}=d$. Using this criterion for contacts we plot the contact time distribution for a set of adhesion parameters in Fig. 10(b). The binary collision peak is still distinctly visible in each distribution and the exponential tail begins at a much later time compared to the corresponding distribution with $d_c=d$ from Fig. 10(a).

In Sec. IV, we will correlate the shift from the Bagnold constitutive relation to the increase in long-time contacts in the flowing pile.

IV. RELATION BETWEEN RHEOLOGY AND CONTACT TIMES

We examine the connection between the contact time distribution and the constitutive relation for the rheology, by identifying correlations between the changing velocity profiles to the contact dynamics in the chute flow. If there exists a simple mapping between some measure of the change in the contact time distribution to changes in the observed rheology, then this distribution can serve as a bridge between the microscopic dynamics at the particle scale to the large-scale collective rheology of the granular continuum. At a minimum, such a measure would allow one to claim that the rheological significance of all of the modifications of the interparticle interactions explored in this paper can be determined solely by their effect on the contact time distribution. Identifying the relevant unifying relation between microscopic mechanics and collective rheology may also serve as the foundation for a better theory relating dynamics across these length scales.

In its simplest form, we seek a single scalar quantity that can be extracted from the contact time distributions. Here we introduce two such measures that characterize the dynamics of (i) anomalously long interparticle contacts, and (ii) typical interparticle contacts of a much shorter duration. We find that the time scale of the atypically long interparticle contact times provides a suitable measure which correlates strongly with changes in the rheology. The typical short-time, collisional contacts bear little insight into deviations from Bagnold scaling. To focus on the long-lived contacts and changes in their duration with variations of the particle interaction parameters, we compute for each simulation the dimensionless number $\dot{\gamma}\tau_l$, which is the product of the inverse shear time with the contact lifetime of a representative set of long-lived contacts chosen by the criterion as follows:

$$P(\tau_l) = 10^{-1}. \tag{13}$$

The contact time distribution is strongly peaked near the two-body collision time with an approximately exponentially

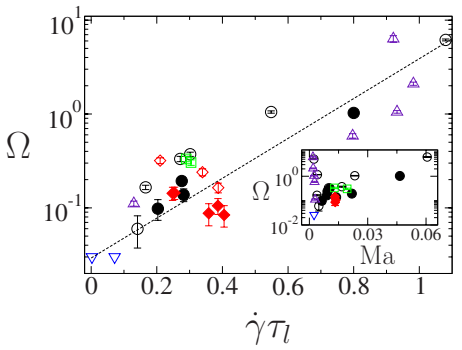

FIG. 11. (Color online) Ω vs $\dot{\gamma}\tau_I$ for a large range of system parameters. Different interaction potentials are specified by open symbols for systems with Hookean interactions and filled symbols for Hertzian interactions. Data is shown for varying k_n (black ○), e_n (red ◇), varying μ (green □), and A for a system with total height $200d$ (purple △). For data where $\Omega \to 0$ (blue ▽), large uncertainties in fitting b prevent determining Ω in these cases, however, these points are included to show that the predicted trend is continued in these limits. The black dashed line is an exponential fit to the data.

decaying tail toward longer contact times. The use of $\dot{\gamma}\tau_I$ effectively quantifies the shift of statistical weight from this short-time peak into the long-time tail.

This measure is clearly not the most obvious to employ; one might, for instance, wish to use a measure of dimensionless contact lifetimes that *reflects the typical dynamics* of the particles such as the Mach number. Since we do not resolve dynamics *within* a single particle, we cannot directly employ this measure, but we expect that the quantity $\mathrm{Ma} = \dot{\gamma} t_{\mathrm{mode}}$ (where t_{mode} is the most probable, two-body contact lifetime) reflects essentially the same short-time-scale dynamics associated with typical intergrain interactions.

Figure 11 shows Ω plotted against $\dot{\gamma}\tau_I$ (measured as described above) on a linear-log scale. We note the nearly monotonic behavior, demonstrating that there is indeed a positive correlation between the value of $\dot{\gamma}\tau_I$ and the breakdown of Bagnold rheology. In fact, we find the empirical relation

$$\Omega = 0.03 e^{4.9 \dot{\gamma}\tau_I} \tag{14}$$

gives an excellent fit of our measure of the deviation from Bagnold rheology as a function of the $\dot{\gamma}\tau_I$, over about two orders of magnitude of variation of Ω. We have checked the robustness of this result by using different values of the threshold for the definition of rare, long-lived contacts [i.e., the value of 10^{-1} on the right-hand side of Eq. (13)]. These different definitions only change the dimensionless constants in the empirical fit. The important aspect of this choice is that the corresponding contact times sufficiently resolve the behavior of the long-lived contact tail of the distribution. This result suggests that the Bagnold relation, while exact in the limit of infinitely hard particles, is, in fact, exponentially sensitive to the growth of long-lived contacts [see Eq. (14)]. These rare events in the granular dynamics appear to control deviations of the collective rheology of the system from the generic Bagnold form.

We note in Fig. 11 that the particle compliance and adhesion are the most dominant parameters of both rheology and contact lifetime statistics. Changing the particle elastic compliance (black ○) generates the largest changes in the rheology. In fact, for stiff enough particles (blue ▽) we cannot detect deviations from Bagnold rheology to the precision of our measurements. Also, if the particles are made very compliant the linear term completely dominates the rheology (data not shown). In both of these limits, the measured $\dot{\gamma}\tau_I$ follows the expected trends, however, these points were not used in fitting the data to Eq. (14) (dashed black line). Interparticle cohesion (purple △) also produces dramatic rheological changes. If d_{eff} is used as the particle contact criterion in the adhesive system, the data also support a simple exponential relation between Ω and $\dot{\gamma}\tau_I$. For the most adhesive system ($A=0.6$), however, we find a significant deviation from this exponential trend. We interpret this result as follows. In this highly cohesive system, about 65% of the system is locked into a solid plug that extends downward from the free surface [25]. Thus the flowing system is significantly smaller and has a greatly reduced shear rate. Near to this stopped regime the shear time increases much faster than the contact lifetimes so that product $\dot{\gamma}\tau_I$ is too small to fit our trend line. Perhaps this point represents the limits of our analysis of the steadily flowing state.

The dissipative parameters—the coefficients of restitution and friction (red ◇ and green □, respectively)—appear to have a negligible effect on both Ω and on the duration of long-lived contacts when scaled by the local shear time. As discussed above, this effect appears to be related to the complementary shifts in both the shear time and contact dynamics that these dissipative parameters generate. Examining these points (the red and green symbols in Fig. 11) more carefully, one notes that there may be a subtle trend opposing our general analysis of the data. As the dissipative parameters are varied to *increase* $\dot{\gamma}\tau_I$, the deviations from the Bagnold constitutive law either remain constant or *slightly decrease*. We do not know if this behavior represents a limitation of the precision of our analysis, or suggests that a single scalar parameter does not control the collective rheology of the system.

In the inset of Fig. 11 we show that there is no similar data collapse when we plot Ω against our version of the Mach number—the typical collision time scaled by the local shear time in the system. The data presented in the inset to Fig. 11 reinforces our idea that deviations away from Bagnold rheology in the densely flowing state are controlled by the duration of atypical, long-lived contacts in the system and not by the most common grain collisional dynamics. This result suggests that deriving the long-time-scale continuum mechanics for systems that are not readily approximated as hard spheres from averages over the microscopic dynamics (as is the typical approach of statistical mechanics) will be very difficult since it appears that the continuum mechanics of the material is strongly influenced by rare events. In this case, the microscopics appears to share similarities with the shear transformation picture [20].

V. SUMMARY

Understanding the relationship between the fundamental interparticle interaction parameters and the larger length-

scale flows of granular materials remains an unsolved problem. In earlier work [25,28] we had proposed a generalized form of the Bagnold constitutive relation to describe the relationship between shear stress and the rate of strain of steady-state, dense granular flow for the inclined plane geometry. This modified Bagnold relation, Eq. (1), consists of the linear combination of two terms: the standard Bagnold term that is quadratic in $\dot{\gamma}$, and a second term that is linear in $\dot{\gamma}$, reminiscent of a usual fluid viscosity. We had found that the presence of interparticle cohesion as might be found in damp granular media [26], leads to a dramatic increase in the linear-in-shear-rate (i.e., viscous) term in the constitutive relation. Based on that work we proposed that the existence of the viscous contribution to momentum transport is due to the presence of long-lived contacts in the system. We noted that, even in our simulations of noncohesive granular media, the Bagnold term accounts for only part of the shear stress in the system. The linear term is also required to explain the flow profiles particularly in the softer particle systems [28].

In this paper we have broadened our analysis of primarily noncohesive granular systems to better explore the constitutive relation of densely flowing sand. We studied a larger parameter space of interparticle interactions by studying the relation of shear stress and rate of strain as a function of particle stiffness, interparticle cohesion, and friction and restitution coefficients. We also studied the effect on the constitutive relation of using the simpler Hookean (linear) interaction between the particles or the more physical Hertzian (nonlinear) force profile. In addition, by changing the inclination angle of the chute, we explored the dependence of these constitutive relations on the overall mean shear rate within the pile for a given set of particle interaction parameters. It is shown that the dimensionless number Ω accounts for the influence of both microscopic (e.g., spring constant) as well as macroscopic (e.g., tilt angle) parameters without appealing to a detailed knowledge of their exact values.

It is found that the prevalence of long contact times as measured by τ_c alone is not sufficient for a change in the granular rheology of the system. Contact times must be measured relative to the local shear time $\dot{\gamma}^{-1}$, which provides the fundamental time scale for the grains during flow. In other words, the lifetime of transient particle structures must be compared to the local frequency of collisions in the bulk, which sets the relevant time scale for momentum transfer. For system parameters that lead to both an increase in the contact times and a decrease in the local shear time, such as k_n and the choice of force laws (Hookean vs Hertzian), strong rheological deviations are observed accompanied by dramatic changes in the dimensionless contact time distributions. For parameters where these time scales are competing, the analysis is considerably more complex. In the case of the dissipative coefficients μ and e_n, any increase in contact times is balanced by a corresponding increase in the shear time for the systems studied here. These parameters do not strongly affect the granular rheology. We also note that a significant fraction of long-lived contacts must be either sliding or stationary in nature since contact times τ_c increase as the coefficient of friction is increased. Finally, we find that deviations from Bagnold rheology when cohesive interactions are included are accurately described only by revising our definition of a "contact" to account for the longer-ranged attractive forces whose influence extends beyond the particle diameter.

We have found that the Bagnold relation, which is exact in the hard-sphere limit, is more robust for elastic particles interacting via a Hookean (linear) force law. For the more physical Hertzian contacts, however, we find that the purely Bagnold constitutive relation poorly represents the rheology for the most elastically compliant particles. In these cases, the flow profile data for chute flow is better described in terms of a standard viscous fluid. This result suggests that experiments performed on elastic particles, such as soft rubber beads and foams [43], will find significant deviations from Bagnold rheology. It is also likely that constitutive relations that neglect particle compliance [14,15] may have to be modified to account for this.

We also present in this paper data suggesting that the role of long-lived interparticle contacts is the primary signal of the breakdown of the Bagnold constitutive law. By examining correlations between the fraction of stress transmitted in the Bagnold (shear rate squared) channel to the viscous one and a simple measure of the change in the contact time distribution in the pile, we find a simple exponential relation between the duration of long-lived contacts $\dot{\gamma}\tau_l$ and deviations from Bagnold rheology as parametrized by Ω. Typical short-time collisions are consistent with the Bagnold picture, but it is only the rare events in the pile that effect deviations from this. We believe that this insight should lead to a more general understanding of the dependence of bulk granular rheology on the microscale grain interactions. This work should guide the development of new theoretical approaches [40] toward connecting microscopic granular mechanics and bulk rheological relations.

ACKNOWLEDGMENTS

R.B. and A.J.L. acknowledge support from NASA Grant No. NRA 02-OB-03-C. Sandia is a multiprogram laboratory operated by Sandia Corporation, a Lockheed Martin Co., for the United States Department of Energy's National Nuclear Security Administration under Contract No. DE-AC04-94AL85000.

[1] C. S. Campbell, Annu. Rev. Fluid Mech. **22**, 57 (1990).
[2] C. Bizon, M. D. Shattuck, J. B. Swift, and H. L. Swinney, Phys. Rev. E **60**, 4340 (1999).
[3] R. M. Nedderman, *Statics and Kinematics of Granular Materials* (Cambridge University Press, Cambridge, 1992).
[4] L. E. Silbert, D. Ertaş, G. S. Grest, T. C. Halsey, D. Levine, and S. J. Plimpton, Phys. Rev. E **64**, 051302 (2001).
[5] C. S. Campbell, J. Fluid Mech. **465**, 261 (2002).
[6] C. S. Campbell, J. Fluid Mech. **539**, 273 (2005).
[7] O. Pouliquen, Phys. Fluids **11**, 542 (1999).
[8] C. Ancey, Phys. Rev. E **65**, 011304 (2001).
[9] T. Borzsonyi and R. E. Ecke, Phys. Rev. E **74**, 061301 (2006).
[10] R. Delannay, M. Louge, P. Richard, N. Taberlet, and A. Valance, Nat. Mater. **6**, 99 (2007).
[11] R. A. Bagnold, Proc. R. Soc. London, Ser. A **225**, 49 (1954); **249**, 235 (1956).
[12] N. Mitarai and H. Nakanishi, Phys. Rev. Lett. **94**, 128001 (2005).
[13] G. Lois, A. Lemaître, and J. M. Carlson, Phys. Rev. E **72**, 051303 (2005).
[14] G. D. R. MiDi, Eur. Phys. J. E **14**, 341 (2004).
[15] F. da Cruz, S. Emam, M. Prochnow, J.-N. Roux, and F. Chevoir, Phys. Rev. E **72**, 021309 (2005).
[16] G. Lois, A. Lemaître, and J. M. Carlson, Phys. Rev. E **76**, 021302 (2007).
[17] G. Lois, A. Lemaître, and J. M. Carlson, Phys. Rev. E **76**, 021303 (2007).
[18] D. Volfson, L. S. Tsimring, and I. S. Aranson, Phys. Rev. E **68**, 021301 (2003).
[19] L. Bocquet, J. Errami, and T. C. Lubensky, Phys. Rev. Lett. **89**, 184301 (2002).
[20] A. Lemaître, Phys. Rev. Lett. **89**, 064303 (2002).
[21] M. Y. Louge, Phys. Rev. E **67**, 061303 (2003).
[22] V. Kumaran, Europhys. Lett. **73**, 232 (2006).
[23] V. Kumaran, J. Fluid Mech. **599**, 121 (2008).
[24] J. T. Jenkins, Phys. Fluids **18**, 103307 (2006).
[25] R. Brewster, G. S. Grest, J. W. Landry, and A. J. Levine, Phys. Rev. E **72**, 061301 (2005). Note: Eq. (6) in this reference is incorrect; the form of the attractive potential in Eq. (5) of this paper is correct and is the attractive potential used in this previous study.
[26] T. C. Halsey and A. J. Levine, Phys. Rev. Lett. **80**, 3141 (1998).
[27] T. G. Mason, A. J. Levine, D. Ertaş, and T. C. Halsey, Phys. Rev. E **60**, R5044 (1999).
[28] L. E. Silbert, G. S. Grest, R. Brewster, and A. J. Levine, Phys. Rev. Lett. **99**, 068002 (2007).
[29] J. Rajchenbach, Eur. Phys. J. E **14**, 367 (2004).
[30] N. Menon and D. J. Durian, Science **275**, 1920 (1997).
[31] P. A. Cundall and O. D. L. Strack, Geotechnique **29**, 47 (1979).
[32] O. R. Walton, Mech. Mater. **16**, 239 (1993).
[33] L. D. Landau and E. M. Lifshitz, *Theory of Elasticity* (Pergamon Press, Oxford, 1986).
[34] D. Ertaş, G. S. Grest, T. C. Halsey, D. Levine, and L. E. Silbert, Europhys. Lett. **56**, 214 (2001).
[35] L. E. Silbert, G. S. Grest, S. J. Plimpton, and D. Levine, Phys. Fluids **14**, 2637 (2002).
[36] X. Jia, C. Caroli, and B. Velicky, Phys. Rev. Lett. **82**, 1863 (1999).
[37] D. Ertaş and T. C. Halsey, Europhys. Lett. **60**, 931 (2002).
[38] L. P. Kadanoff, Rev. Mod. Phys. **71**, 435 (1999).
[39] N. Mitarai and H. Nakanishi, Phys. Rev. E **67**, 021301 (2003).
[40] R. Brewster and A. J. Levine (unpublished).
[41] G. Lois, A. Lemaître, and J. M. Carlson, Europhys. Lett. **76**, 318 (2006).
[42] L. E. Silbert, Phys. Rev. Lett. **94**, 098002 (2005).
[43] D. J. Durian, Phys. Rev. Lett. **75**, 4780 (1995).